

# Instability of the roll/streak structure induced by free-stream turbulence in pre-transitional Couette flow

Brian F. Farrell

*School of Engineering and Applied Science, Harvard University*

Petros J. Ioannou\* and Marios-Andreas Nikolaidis

*Department of Physics, National and Kapodistrian University of Athens*

(Dated: March 13, 2017)

Although the roll/streak structure is ubiquitous in both observations and simulations of pre-transitional wall-bounded shear flow, this structure is linearly stable if the idealization of laminar flow is made. Lacking an instability, the large transient growth of the roll/streak structure has been invoked to explain its appearance as resulting from chance occurrence in the background turbulence of perturbations configured to optimally excite it. However, there is an alternative interpretation for the role of free-stream turbulence in the genesis of the roll/streak structure which is that the background turbulence interacts with the roll/streak structure to destabilize it. Statistical state dynamics (SSD) provides analysis methods for studying instabilities of this type which arise from interaction between the coherent and incoherent components of turbulence. Stochastic structural stability theory (S3T), which implements SSD in the form of a closure at second order, is used in this work to analyze the SSD modes arising from interaction between the coherent streamwise invariant component and the incoherent background component of turbulence. In pre-transitional Couette flow a manifold of stable modes with roll/streak form is found to exist in the presence of low intensity background turbulence. The least stable mode of this manifold is destabilized at a critical value of a parameter controlling the background turbulence intensity and a finite amplitude roll/streak structure arises from this instability through a bifurcation in this parameter. Although this bifurcation has analytical expression only in SSD, it is closely reflected in both the dynamically similar quasi-linear system, referred to as the restricted non-linear (RNL) system, and in DNS. This correspondence is verified using ensemble implementations of the RNL and DNS systems. S3T also predicts a second bifurcation at a higher value of the turbulent excitation parameter that results in destabilization of the finite amplitude roll/streak equilibria. This second bifurcation is shown to lead first to time dependence of the roll/streak in the S3T system and then to chaotic fluctuation corresponding to minimal channel turbulence. This transition scenario is also verified in simulations of the RNL and DNS systems. Bifurcation from a finite amplitude roll/streak equilibrium provides a direct route to the turbulent state through the S3T roll/streak instability.

## I. INTRODUCTION

Streamwise roll vortices and associated streamwise streaks were identified in experiments on transition in boundary layers [1] and observed in the near wall region of turbulent flows [2–4]. These observations were subsequently corroborated by direct numerical simulations (DNS) (cf. Kim *et al.* [5]) and the roll/streak structure is now understood to be central to the dynamics of turbulence in wall-bounded shear flows.

There are two distinct dynamical problems central to understanding wall-turbulence: transition from the laminar to the turbulent state and maintenance of the turbulent state. The roll/streak structure, despite being hydrodynamically stable, is commonly agreed to be involved in instigating transition from the laminar to the turbulent state in these flows. After transition this structure persists but becomes highly variable in both space and time. This time-dependent streamwise roll and streak structure is believed to be involved in the process

maintaining turbulence in shear flow that is referred to as the self-sustaining process [6–9]. Moreover, this self-sustaining mechanism appears to be quite general in that it operates not only in the near-wall region but also, and independently, in the logarithmic layer [10, 11].

Our primary interest in this work is in the robust observation of the roll/streak structure in wall-bounded shear flow prior to transition and in understanding the role of this structure in the transition process. The prominence of the roll/streak in these flows presents a problem because this structure is not an unstable eigenmode of the shear flow existing prior to transition. The robust observation of the roll/streak structure was first rationalized by appeal to the lift-up mechanism which describes the kinematic conversion of wall normal velocity into streamwise streak velocity in sheared flows [12, 13]. This insight was later advanced by recognition that the lift-up mechanism could be subsumed into the analytical structure of generalized stability theory (GST) by which modal stability theory and non-normal transient growth analysis are united [14–16]. While modal stability analysis provides no reason to expect appearance of roll/streak structures, GST analysis predicts optimally growing perturbations with the observed form [17, 18].

---

\* pjioannou@phys.uoa.gr

The success of optimal growth theory in predicting the roll/streak structure observed in perturbed wall-bounded shear flow prior to transition appeared at first to be persuasive that the explanation for observations of this structure in pre-transitional flow was secure. Nevertheless, there remained a lingering doubt. For one thing, there is the regularity of the spacing and amplitude of the roll/streak in experiments [19, 20], which, as remarked by Townsend [21], is characteristic of modal growth. And then there is the observation that streamwise rolls decay in amplitude if background turbulence levels are sufficiently low, consistent with predictions based on transiently growing optimals [22–24], while rolls grow downstream in the presence of moderate levels of background turbulence intensity [25], which is incompatible with transient growth and suggestive of an underlying unstable mode.

While the absence of roll/streak instability in an unperturbed wall-bounded shear flow is established, pseudospectral theory [26, 27] reveals that a highly non-normal operator, such as that of Navier-Stokes (NS) dynamics linearized about a strongly sheared flow, can be destabilized by small perturbations to the dynamical operator itself. Consistently, it was recently shown that an emergent instability with roll/streak structure arises from interaction between the roll/streak structure and a field of background turbulence with sufficient amplitude [28]. This instability does not have analytical expression in the linearized NS dynamics of the laminar flow because it is not a linear instability of the laminar shear flow but instead arises from systematic organization by the roll/streak structure of the Reynolds stress associated with the incoherent background turbulence. The analytical expression for this instability therefore exists only in the equations for the associated statistical state dynamics (SSD). The formulation of SSD used in this work to study this instability, referred to as S3T, is a second order closure of the Navier-Stokes dynamics (NS) in which full nonlinearity is retained in the streamwise mean equation (first cumulant) while the dynamics of the perturbation covariance (second cumulant) is linearized about the instantaneous streamwise mean flow. Nonlinear interaction occurs between the mean flow dynamics (defined as flow components with streamwise wavenumber  $k_x = 0$ ) and the perturbation covariance obtained from flow components with streamwise wavenumber  $k_x \neq 0$ , while nonlinearity is parameterized by a stochastic excitation in the perturbation dynamics rather than being explicitly calculated. This quasi-linear formulation in which nonlinearity is parameterized in the perturbation dynamics is referred to as the restricted nonlinear (RNL) approximation to the full nonlinear Navier-Stokes dynamics (NL). In this work we use RNL to construct finite ensemble approximations to the equivalently infinite ensemble of the S3T version of SSD. Consistent with this usage, the perturbation equations making up the ensemble in an RNL-based approximation to S3T are used only to calculate an approximate covariance. As a consequence phase in-

formation is not retained for the perturbation fields, only their second order correlations being relevant to a second order SSD.

As alluded to above, the approximation to the perturbation covariance obtained using RNL dynamics can be systematically improved by forming a mean covariance from an ensemble of RNL perturbation equations sharing a single mean flow. In the case that an  $N$ -member ensemble is used to approximate the covariance the SSD approximation is referred to as  $\text{RNL}_N$  [29]. In the limit  $N \rightarrow \infty$  S3T dynamics is recovered. RNL has the advantage that it can be easily implemented at high resolution while retaining the analytical restrictions of S3T. Moreover, simulations made using RNL can be compared to the same DNS implementation that was restricted to obtain the RNL system [11, 30].

Further insight can be obtained by proceeding similarly with the NS equations by formally writing the full dynamics in mean/perturbation form and then calculating an ensemble average second order closure using an  $N$ -member ensemble of perturbation equations sharing a single mean flow in a manner parallel to the method used in constructing  $\text{RNL}_N$  but retaining full nonlinearity in the individual perturbation equations of the ensemble. This closure will be referred to as  $\text{NL}_N$ . When it converges  $\text{NL}_N$  corresponds to a complete cumulant expansion of the SSD solved up to second order. We find that in our example problem satisfactory convergence of  $\text{RNL}_N$  and  $\text{NL}_N$  is obtained for  $N$  as small as 10.

Consider a Couette flow subjected to a random excitation that is statistically streamwise and spanwise homogeneous and has zero mean with respect to time and space averaging. S3T predicts a bifurcation occurring at a critical amplitude of the excitation in which an unstable roll/streak structure emerges as an instability of the S3T dynamics. It is important at this point to be clear about what entity is being referred to as unstable. The unstable mode we are studying arises as an eigenmode with roll/streak structure at infinitesimal amplitude that eventually grows sufficiently to become a nonlinearly equilibrated finite amplitude equilibrium that retains roll/streak structure. The existence of coherent roll/streak structures in the flow is therefore explained by the growth and equilibration of this unstable mode. It is perhaps more correct to say that the flow is unstable to this roll/streak structure than to say that this roll/streak structure is unstable, which would admit the alternative interpretation that the finite amplitude roll/streak structure is itself unstable. At sufficiently high background turbulence levels the finite amplitude roll/streak structure proceeding from the S3T unstable mode does become itself subject to secondary instability leading to transition to a self-sustaining turbulent state as we will show. The perturbative S3T instability connects directly to the finite amplitude roll/streak structure which becomes secondarily unstable, but these secondary instabilities are not of roll/streak form. There is an analogy between equilibrated finite amplitude roll/streak struc-

tures in S3T and exact coherent structures in laminar flow [31–36], although exact coherent structures are finite amplitude isolated equilibria that do not connect to infinitesimal instabilities of the spanwise independent laminar flow as the S3T roll/streak structures do. While S3T finite amplitude roll/streak structures become secondarily unstable only when these roll/streak reaches high amplitude under excitation by strong background turbulence, the isolated exact coherent structures generally support secondary instabilities, for example those discussed in Deguchi & Hall [36, 37] in their investigation of the stability of the finite amplitude states in vortex-wave interaction theory (VWI). We remark that once its secondary instability becomes supported the coherent equilibrium S3T roll/streak structure is rapidly destroyed. This observation suggests that physically realistic levels of background turbulence should excite the parasitic modes of exact coherent structures as well. In order to maintain such unstable structures it is necessary to eliminate naturally occurring sources of perturbations that would necessarily excite the parasitic modes to which these structures are vulnerable. In contrast, the S3T instability results from organization of the background disturbances which constitutes its energy source so rather than being detrimental to it, the S3T mode growth rate increases with increasing background disturbance amplitude.

Returning now to the S3T instabilities with roll/streak form; as the background turbulence excitation is increased, at first the streamwise and spanwise averaged mean flow differs little from the laminar Couette profile while superimposed on this profile is a fixed point finite amplitude roll/streak structure. With further increase in the excitation amplitude another critical value is exceeded at which the flow transitions to turbulence. The existence of these three statistical regimes under increasing levels of background turbulence: the near laminar state, the near laminar with superimposed finite amplitude equilibrated roll/streak structure, and the turbulent regime characterized by chaotic fluctuation of the roll/streak structure in Couette flow was predicted using S3T [28]. The purpose of this paper is to determine whether these predictions made using S3T are reflected in ensemble RNL and NL SSD approximations and to analyze the convergence to the S3T predictions obtained using the RNL<sub>N</sub> and NL<sub>N</sub> approximations as  $N \rightarrow \infty$ .

## II. FORMULATION OF S3T

Consider a plane Couette flow with streamwise direction  $x$ , wall-normal direction  $y$  and spanwise direction  $z$  in which background turbulence is maintained by stochastic excitation applied throughout the flow. The lengths of the channel in the streamwise, wall-normal and spanwise direction are respectively  $L_x$ ,  $2h$  and  $L_z$ . The channel walls are at  $y/h = -1$  and  $1$ . Spatial and temporal averages are denoted by square brackets

with a subscript denoting the independent variable over which the average is taken, i.e. spanwise averages by  $[\cdot]_z = L_z^{-1} \int_0^{L_z} \cdot dz$ , time averages by  $[\cdot]_t = T^{-1} \int_0^T \cdot dt$ , with  $T$  sufficiently long. Multiple subscripts denote an average over the subscripted variables in the order they appear, i.e.  $[\cdot]_{x,y} \stackrel{\text{def}}{=} [[\cdot]_x]_y$ . The vector velocity  $\mathbf{u}$  is decomposed into its streamwise mean, denoted by  $\mathbf{U}(y, z, t) \stackrel{\text{def}}{=} [\mathbf{u}(x, y, z, t)]_x$ , and the deviation from this mean (the perturbation) denoted  $\mathbf{u}'(x, y, z, t)$  so that  $\mathbf{u} = \mathbf{U} + \mathbf{u}'$ . The pressure gradient is similarly decomposed as  $\nabla p = \nabla (P(y, z, t) + p'(x, y, z, t))$ . Velocity is non-dimensionalized by the velocity at the wall,  $U_w$ , at  $y/h = 1$ , lengths by  $h$ , and time by  $h/U_w$ . The non-dimensional NS equations decomposed into an equation for the mean and an equation for the perturbation are:

$$\partial_t \mathbf{U} + \mathbf{U} \cdot \nabla \mathbf{U} + \nabla P - \Delta \mathbf{U} / R = -[\mathbf{u}' \cdot \nabla \mathbf{u}']_x, \quad (1a)$$

$$\begin{aligned} \partial_t \mathbf{u}' + \mathbf{U} \cdot \nabla \mathbf{u}' + \mathbf{u}' \cdot \nabla \mathbf{U} + \nabla p' - \Delta \mathbf{u}' / R = \\ = -(\mathbf{u}' \cdot \nabla \mathbf{u}' - [\mathbf{u}' \cdot \nabla \mathbf{u}']_x) + \sqrt{\varepsilon} \mathbf{f}', \end{aligned} \quad (1b)$$

$$\nabla \cdot \mathbf{U} = 0, \quad \nabla \cdot \mathbf{u}' = 0, \quad \nabla \cdot \mathbf{f} = 0 \quad (1c)$$

where  $R = U_w h / \nu$  is the Reynolds number. The velocities and the stochastic excitation  $\mathbf{f}'(x, y, z, t)$  satisfy periodic boundary conditions in the  $z$  and  $x$  directions and no-slip boundary conditions in the cross-stream direction:  $\mathbf{U}(x, \pm 1, z, t) = (\pm 1, 0, 0)$ ,  $\mathbf{u}'(x, \pm 1, z, t) = \mathbf{f}'(x, \pm 1, z, t) = 0$ . The stochastic excitation is applied only to the streamwise varying Fourier components of the flow. It is nondivergent, has zero ensemble mean,  $\langle \mathbf{f}' \rangle = 0$  (the ensemble mean over excitation realizations being denoted  $\langle \cdot \rangle$ ), and is delta correlated in time and statistically homogeneous in the  $x$  and  $z$  directions. Delta correlation in time of the excitations implies that the energy input by the stochastic excitation is independent of the flow state and can be parameterized by  $\varepsilon$  in (1b). The  $x, y, z$  components of  $\mathbf{U}$  are  $(U, V, W)$  and the corresponding components of  $\mathbf{u}'$  are  $(u', v', w')$ . The streak component of the streamwise mean flow is denoted by  $U_s$  and defined as

$$U_s \stackrel{\text{def}}{=} U - [U]_z. \quad (2)$$

The streamwise mean cross-stream and spanwise velocities,  $V$  and  $W$ , are found to primarily constitute the roll vortices. We also define the streak energy density,  $E_s = [U_s^2/2]_{y,z}$ , the roll energy density,  $E_r = [(V^2 + W^2)/2]_{y,z}$ , and the perturbation energy density  $E_p = [|\mathbf{u}'|^2/2]_{x,y,z}$ . Energy is injected from the moving walls at rate  $I = (2R)^{-1} [\partial_y U|_{y=1} + \partial_y U|_{y=-1}]_z$  and at rate  $\varepsilon$  from the appropriately normalized stochastic forcing. Energy is dissipated at rate  $D = R^{-1} [|\nabla \times \mathbf{u}|^2]_{x,y,z}$ . With  $I_c$  and  $D_c$  we denote the energy injection and dissipation rates of the Couette flow.

The S3T dynamics is a SSD governing the evolution of the first two cumulants consisting of the streamwise

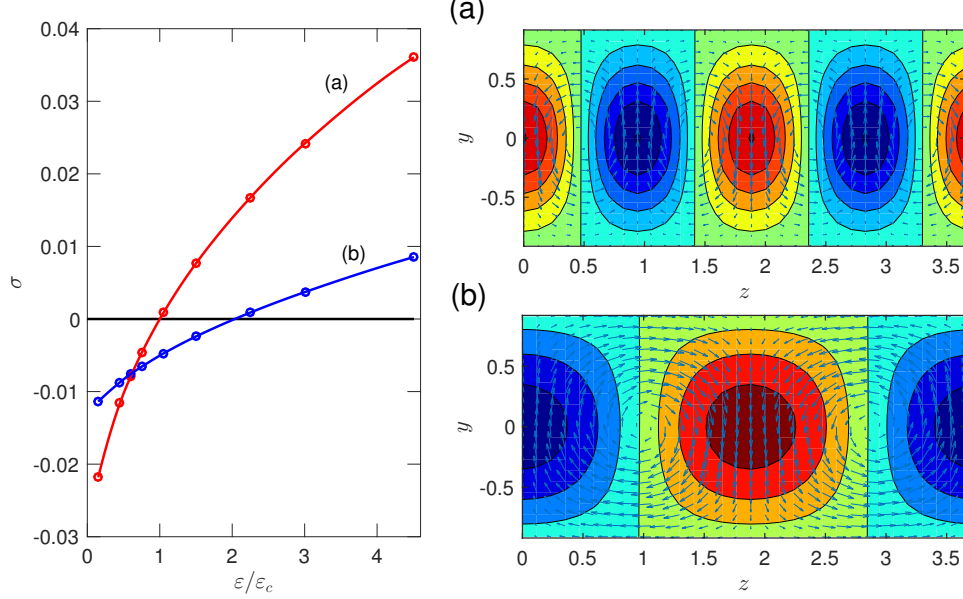


FIG. 1: Left: Growth rate of the two most unstable S3T eigenfunctions about the spanwise homogeneous S3T equilibrium as a function of the excitation amplitude of the background turbulence,  $\varepsilon$ . Right: The structure of the corresponding eigenfunctions with growth rate (a) and (b) for excitation amplitude  $\varepsilon/\varepsilon_c = 2$ . Shown are contours of the streak velocity,  $U_s$ , and velocity vectors of the components  $(V, W)$  plotted on a  $(y, z)$  plane cross-section. The structure of these eigenfunctions does not change appreciably for  $\varepsilon/\varepsilon_c < 6$ . At  $\varepsilon = \varepsilon_c$  the S3T spanwise uniform equilibrium bifurcates to a finite amplitude equilibrium with perturbation structure close to that of the most unstable eigenfunction shown in (a). The channel is minimal with  $L_x = 1.75\pi$  and  $L_z = 1.2\pi$ , the Reynolds number is  $R = 400$ , and the stochastic forcing excites only Fourier components with streamwise wavenumber  $k_x = 2\pi/L_z = 1.143$ . The critical  $\varepsilon_c$  sustains a background turbulent field with mean energy 0.14% of the Couette flow energy.

mean flow,  $\mathbf{U} = (U, V, W)$  or  $\mathbf{U} \stackrel{\text{def}}{=} (U_x, U_y, U_z)$ , and the second cumulants that are the same time covariances of the Fourier components of the velocity fluctuations,  $\hat{u}'_{\alpha, k_x}$ , where the index  $\alpha = x, y, z$  indicates the velocity component in the Fourier expansion of the perturbation velocity  $\mathbf{u}'$ :

$$\mathbf{u}'(x, y, z, t) = \sum_{k_x > 0} \text{Re} \left( \hat{\mathbf{u}}'_{k_x}(y, z, t) e^{ik_x x} \right), \quad (3)$$

with  $k_x$  the streamwise wavenumbers that are excited by the stochastic excitation. We similarly expand the excitation in its Fourier components  $\hat{\mathbf{f}}'_{k_x}$ . In this study we will limit the stochastic excitation to only the streamwise fundamental wavenumber  $k_x = 2\pi/L_x$  and as a result the subscript  $k_x$  in the velocity and excitation components can be dropped without ambiguity. Because in the S3T equations the perturbation-perturbation interactions are not included, this choice of excitation implies that the S3T flow field perturbations have power only at the streamwise component that is forced. The covariance variables of S3T are the covariances of the velocity components of Fourier component  $k_x$  between point 1  $\stackrel{\text{def}}{=} (y_1, z_2)$  and point 2  $\stackrel{\text{def}}{=} (y_2, z_2)$  evaluated at the same

time:

$$C_{\alpha\beta}(1, 2) = \langle \hat{u}'_{\alpha}(1) \hat{u}'_{\beta}^*(2) \rangle, \quad (4)$$

which is a function of the coordinates of the two points (1) and (2) on the  $(y, z)$  plane and of time (\* denotes complex conjugation). The S3T equations are:

$$\begin{aligned} \partial_t U_{\alpha} + U_{\beta} \partial_{\beta} U_{\alpha} + \partial_{\alpha} P - \Delta U_{\alpha} / R = \\ = -\frac{1}{2} \text{Re} \left( \partial_y C_{y\alpha}(1, 1) + \partial_z C_{z\alpha}(1, 1) \right), \end{aligned} \quad (5a)$$

$$\begin{aligned} \partial_t C_{\alpha\beta}(1, 2) = A_{\alpha\gamma}(1) C_{\gamma\beta}(1, 2) \\ + A_{\beta\gamma}^*(2) C_{\alpha\gamma}(1, 2) + Q_{\alpha\beta}(1, 2), \end{aligned} \quad (5b)$$

$$\partial_a U_a = 0, \quad \hat{\partial}_{\alpha}(1) C_{\alpha\beta}(1, 2) = \hat{\partial}_{\beta}^*(2) C_{\alpha\beta}(1, 2) = 0, \quad (5c)$$

with summation convention on repeated indices and the operator  $\hat{\partial} \stackrel{\text{def}}{=} (ik_x, \partial_y, \partial_z)$  (for a derivation cf. [28]). The operator  $A_{\alpha\beta}(1)$  (or  $A_{\alpha\beta}(2)$ ) is the operator governing the quasi-linear evolution of streamwise varying perturbations in (1b) with streamwise wavenumber  $k_x = 2\pi/L_x$  linearized about the instantaneous streamwise mean flow  $\mathbf{U}(1)$  (or  $\mathbf{U}(2)$ ) and 1 (or 2) indicates that the operator



acts on the 1 (or the 2) variable of  $C(1, 2)$ .  $Q_{\alpha\beta}(1, 2)$  are the spatial covariances of the  $k_x$  Fourier components of the forcing components,  $\hat{f}_i$ , and are defined as

$$\langle \hat{f}_\alpha(1, t_1) \hat{f}_\beta^*(2, t_2) \rangle = \delta(t_1 - t_2) Q_{\alpha\beta}(1, 2). \quad (6)$$

Using S3T we can find roll/streak structures that are independent of time because their forcing derives from a converged covariance obtained from an equivalently infinite ensemble of independent realizations. These fixed point equilibria are imperfectly reflected in individual realizations because fluctuations in the covariance arise due to the finiteness of the equivalent ensemble of statistically independent structures that fit in the channel. These fluctuations in the covariance result in imperfect correspondence with the underlying equilibrium structure revealed by S3T (cf. [38, 39]). In order to verify that the S3T fixed point does in fact underly the dynamics of the roll/streak structure observed in RNL and NS it is useful to obtain solutions lying on the continuum from the single realization solution to the infinite ensemble S3T fixed point solution. S3T dynamics is approached by  $\text{RNL}_N$  simulations as  $N \rightarrow \infty$ . The  $\text{RNL}_N$  system is governed by the system of equations

$$\partial_t \mathbf{U} + \mathbf{U} \cdot \nabla \mathbf{U} + \nabla P - \Delta \mathbf{U} / R = - \langle [\mathbf{u}' \cdot \nabla \mathbf{u}']_x \rangle_N, \quad (7a)$$

$$\partial_t \mathbf{u}'_n + \mathbf{U} \cdot \nabla \mathbf{u}'_n + \mathbf{u}'_n \cdot \nabla \mathbf{U} + \nabla p'_n - \Delta \mathbf{u}'_n / R = \sqrt{\varepsilon} \mathbf{f}'_n, \quad (7b)$$

$$\nabla \cdot \mathbf{U} = 0, \quad \nabla \cdot \mathbf{u}'_n = 0, \quad \nabla \cdot \mathbf{f}'_n = 0 \quad (7c)$$

where  $n = 1, \dots, N$  indicates the ensemble member, and  $\langle \cdot \rangle_N$  indicates an average over the  $N$  ensemble members. Note that in correspondence with S3T dynamics the perturbation-perturbation interaction in (1b) is ignored.

In a similar manner we can define ensemble  $\text{NL}_N$  simulations correspond to the first two components of a converged expansion in cumulants.  $\text{NL}_N$  is governed by the system of equations:

$$\partial_t \mathbf{U} + \mathbf{U} \cdot \nabla \mathbf{U} + \nabla P - \Delta \mathbf{U} / R = - \langle [\mathbf{u}' \cdot \nabla \mathbf{u}']_x \rangle_N, \quad (8a)$$

$$\begin{aligned} \partial_t \mathbf{u}'_n + \mathbf{U} \cdot \nabla \mathbf{u}'_n + \mathbf{u}'_n \cdot \nabla \mathbf{U} + \nabla p'_n - \Delta \mathbf{u}'_n / R = \\ = - (\mathbf{u}'_n \cdot \nabla \mathbf{u}'_n - [\mathbf{u}'_n \cdot \nabla \mathbf{u}'_n]_x) + \sqrt{\varepsilon} \mathbf{f}'_n, \end{aligned} \quad (8b)$$

$$\nabla \cdot \mathbf{U} = 0, \quad \nabla \cdot \mathbf{u}'_n = 0, \quad \nabla \cdot \mathbf{f}'_n = 0 \quad (8c)$$

We are interested in whether the analytical predictions of the S3T equations are approached in  $\text{RNL}_N$  and  $\text{NL}_N$  simulations as  $N$  increases. Results are presented for the minimal Couette flow channel of Hamilton, Kim & Waleffe [7] at  $R = 400$  (based on channel half-width) with streamwise length  $L_x = 1.75\pi$ , spanwise length  $L_z = 1.2\pi$  and channel half-width  $L_y = 1$ . The gravest

streamwise wavenumber  $k_x = 2\pi/L_x$  is stochastically excited using independent compact support cross-stream velocity and cross-stream vorticity structures in  $(y, z)$ . Numerical calculations employ  $N_y = 21$  grid points in the cross-stream direction and 32 harmonics in the spanwise and streamwise directions. Other stochastic excitations produce only qualitative differences in the results. A study of the S3T dynamics of this channel model was reported in [28].

### III. COMPARISON OF ROLL/STREAK BIFURCATION AND STRUCTURE IN S3T, $\text{RNL}_N$ AND $\text{DNS}_N$

The S3T SSD (5) supports spanwise uniform fixed point solutions with streamwise mean flow form  $\mathbf{U}_e = (U_e(y), 0, 0)$  and associated spanwise covariance  $C_e(y_1, y_2, z_1 - z_2)$ . Taking  $\varepsilon = 0$ , recovers the laminar Couette flow  $U_e = y$  with  $C_e = 0$ . As  $\varepsilon$  increases the equilibrium streamwise mean flow,  $U_e(y)$ , departs from the Couette flow. Stability of these spanwise uniform S3T equilibria can be determined as a function of  $\varepsilon$  using the S3T equations (5) linearized about these fixed points [28].

Eigenvalues and the associated mean flow eigenfunction structure for the first two most unstable S3T modes are shown in Fig. 1. The complete associated eigenfunctions comprise both a mean flow component ( $\delta U(y, z), \delta V(y, z), \delta W(y, z)$ ), which is shown in Fig. 1, and a covariance component  $\delta C(y_1, y_2, z_1, z_2)$ . The structure of the mean flow component of these eigenfunctions changes only slightly as the amplitude of the forcing,  $\varepsilon$ , increases. The eigenfunctions consist of low and high speed streamwise streaks together with roll circulations exactly collocated to reinforce the streak velocity. Despite being more highly dissipated by diffusion, the mean flow eigenfunction which becomes unstable first as  $\varepsilon$  increases is not the eigenstructure with the gravest spanwise wavenumber  $k_z = 2\pi/L_z = 1.67$ , shown in Fig. 1b, but the second spanwise harmonic with wavenumber  $k_z = 4\pi/L_z = 3.33$ , shown in Fig. 1a. Destabilization of these roll/streak eigenfunctions can be traced to a universal positive feedback mechanism operating in turbulent flows: when incoherent turbulence is perturbed by a coherent streak, the streak distorts the incoherent turbulence so as to induce ensemble mean Reynolds stresses forcing streamwise mean roll circulations configured to reinforce the streak perturbation that gave rise to them (cf. [28]). The modal streak perturbations of the fastest growing eigenfunctions induce the strongest such feedback (when account has been taken for viscous damping).

We note that neutral mode and critical layer based self-sustaining process (SSP) theories such as the vortex-wave interaction theory (VWI) predict structures at variance with the S3T unstable modes we obtain. As shown in Fig. 1a,b organization of the Reynolds stress by the streak (even at perturbational amplitude) results in a

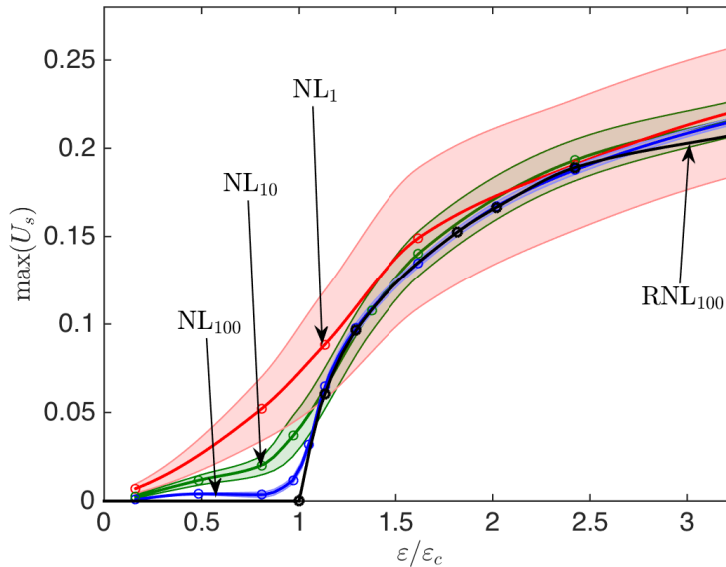


FIG. 2: Bifurcation diagram for the Couette problem. Shown is the time mean of the maximum value of the streak amplitude,  $U_s$  as a function of the stochastic excitation amplitude,  $\epsilon$ , for an  $NL_1$  simulation (red), an ensemble  $NL_{10}$  simulation (green), an ensemble  $NL_{100}$  simulation (blue), and an ensemble  $RNL_{100}$  simulation (black). The critical bifurcation value has been determined from stability analysis of the S3T system and it has been confirmed that this value is closely approximated using  $RNL_{100}$ . For  $\epsilon/\epsilon_c < 1$ , S3T predicts that the streamwise streak and roll amplitude is zero. At  $\epsilon = \epsilon_c$  the S3T spanwise uniform equilibrium bifurcates giving rise to a finite amplitude equilibrium with roll and streak. The  $NL_1$  and  $NL_{10}$  simulations exhibit fluctuating streak/roll structures and one standard deviation of the fluctuations correspond to the shaded regions in the figure. The fluctuations in the ensemble  $NL_{100}$  and  $RNL_{100}$  simulations are small and only those associated with  $NL_{100}$  are shown. Other parameters as in Fig. 1.

smooth domain-wide forcing of the roll circulation. At high Reynolds number in the neutral mode SSP and VWI mechanisms this interaction is localized at the critical layer [32, 34, 36, 40]. The interaction between perturbations and mean flow in neutral mode and VWI theories by necessity occurs near the critical layer in the inviscid limit because according to the non-acceleration theorem at steady state and in the absence of forcing and dissipation there is no interaction between mean and perturbations except at the critical layer [41–43]. In S3T there is forcing and consequently the interaction is not required to be concentrated in the vicinity of the critical layer. The modes we calculate organize distributions of Reynolds stress with divergence exactly coherent with the mode roll structure, as is required of a mode solution, and not in any sense concentrated at a critical surface. In fact the lack of any evidence for concentration of Reynolds stress divergence at a particular cross-stream location either in our stable roll/streak regime or in our self-sustaining turbulence simulations argues against a mechanism relying on an interaction localized at a critical surface.

S3T stability analysis determines the critical excitation,  $\epsilon_c$ , at which the spanwise homogeneous turbulent equilibrium state becomes unstable. For the parameters

of our example problem this  $\epsilon_c$  corresponds to maintaining in the Couette flow a perturbation field with mean energy density 0.14% of the energy density of the Couette flow. For  $\epsilon > \epsilon_c$  a symmetry breaking occurs with the emergence of mean flow structures in the form of the fastest growing eigenfunction which is shown in Fig. 1a. Over a finite interval  $\epsilon_c < \epsilon < \epsilon_t$  the unstable S3T eigenfunction equilibrates nonlinearly to form finite amplitude S3T equilibria with roll/streak structure qualitatively similar to the corresponding eigenfunction (for our examples  $\epsilon_t/\epsilon_c \approx 5.5$ ).

A bifurcation diagram showing the maximum of the streak velocity,  $U_s$ , and of the streamwise mean cross-stream velocity,  $V$ , is shown as a function of  $\epsilon$  in Fig. 2. The indicated critical  $\epsilon_c$  was determined by S3T stability analysis. For  $\epsilon/\epsilon_c < 1$  the equilibrium is spanwise independent with no coherent roll/streak structure. The equilibrium values shown in Fig. 2 were obtained using  $RNL_{100}$  simulations. These  $RNL_{100}$  equilibria have been verified to be very close to the infinite ensemble S3T equilibria.

Single NL and ensemble NL integrations allow us to study the correspondence between the infinite ensemble predictions of S3T analysis and NL turbulence. While finite ensemble simulations produce fluctuating roll/streak

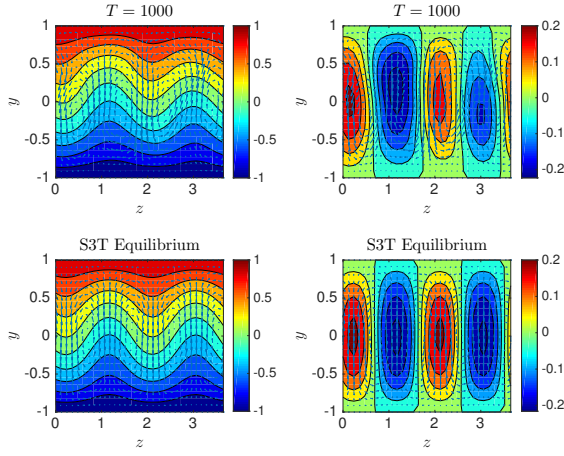


FIG. 3: Top panels: Snapshot of the streamwise mean flow from an  $NL_1$  simulation at stochastic excitation amplitude  $\varepsilon/\varepsilon_c = 3$ . Shown are contours of the streamwise mean velocity  $U$  (left top), streak velocity,  $U_s$  (right top) and velocity vectors of the components  $(V, W)$  in the  $(y, z)$  plane at  $t = 1000$  of the simulation. Bottom panels: The corresponding streamwise mean flow for the S3T system at  $\varepsilon/\varepsilon_c = 3$ . This figure shows that the equilibrium roll/streak regime predicted by S3T is reflected in single realizations of the NL equations. The development of the roll/streak structure in a  $NL_1$  simulation can be seen in MOVIE1 (cf. supplementary materials). The development of the roll/streak equilibrium in a S3T equilibrium simulation can be seen in MOVIE2 (cf. supplementary materials). Parameters are as in the previous figures.

structures we find that even in the case of a realization simulation, corresponding to  $N = 1$ , a clear roll/streak structure emerges for  $\varepsilon > \varepsilon_c$  which exhibits great persistence and has the same structure as that predicted by S3T analysis. An indicative comparison between an S3T equilibrium roll/streak structure and a snapshot of the corresponding roll/streak from an  $NL_1$  simulation at  $\varepsilon/\varepsilon_c = 3$  is shown in Fig. 3.

While the S3T equilibria are fixed points, the corresponding roll/streak structure in the  $NL_1$  simulation reflect the time independence of the S3T equilibria imperfectly. However, it is persuasive that the analytical structure revealed by S3T analysis underlies the behavior seen in the  $NL_1$  simulation; for example see the snapshots shown in Fig. 4. Noise driven fluctuations of the ensemble structure are also apparent in the bifurcation diagram shown in Fig. 2 in which the mean and variance of the maximum streak,  $U_s$ , in  $NL_1$  and  $NL_{10}$  are indicated. The reflection of the analytical S3T bifurcation is clearly seen in the  $NL_{10}$  results and near convergence is obtained in the  $NL_{100}$  results.

We have demonstrated that the unstable roll/streak modes and associated finite amplitude S3T equilibria

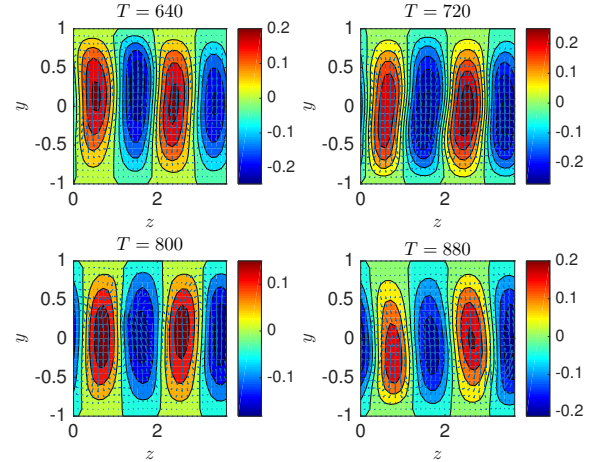


FIG. 4: Snapshots at times  $t = 640, 720, 800, 880$  of the contours of the streak velocity,  $U_s$ , and velocity vectors of the components  $(V, W)$  plotted on a  $(y, z)$  plane cross-section from an  $NL_1$  simulation at stochastic excitation amplitude  $\varepsilon/\varepsilon_c = 3$ . This figure shows the persistence of the organized structure in  $NL_1$ . This structure and its persistence stem from the underlying equilibrium state that exists for this excitation amplitude in the S3T dynamics. The other parameters are as in the previous figures.

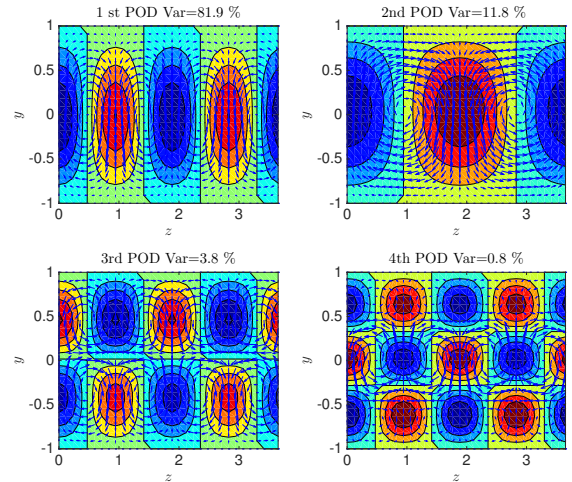


FIG. 5: Contours of streak velocity,  $U_s$ , and vectors of roll components  $(V, W)$  plotted on a  $(y, z)$  cross-section for the first 4 PODs of the streamwise mean flow fluctuations of an  $NL_1$  forced at  $\varepsilon/\varepsilon_c = 0.75$ . The PODs come in pairs. The first pair of PODs which account for 82% of the energy of the fluctuations of the streamwise mean flow has the structure of the least damped S3T mode which because of the synergistic mechanism revealed by S3T is not the gravest mode in the channel. This figure shows that the fluctuations in the  $NL_1$  simulations reveal the S3T stable modes. Other parameters as in the previous figures.

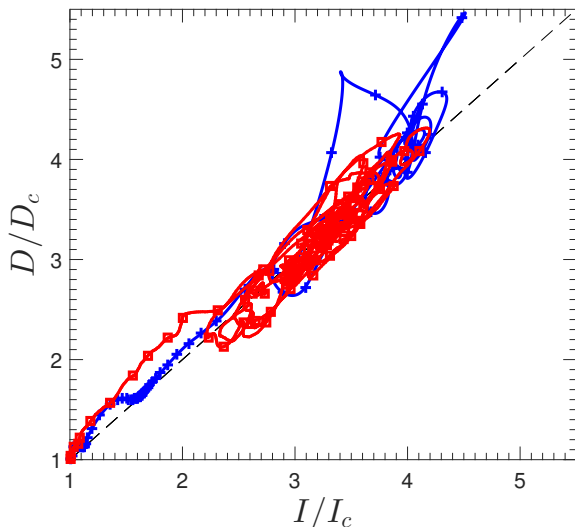


FIG. 6: Evolution of energy input rate,  $I/I_c$  and dissipation rate,  $D/D_c$ , from the laminar state to the turbulent state in an  $NL_1$  simulation (squares-solid) and in an S3T simulation (crosses-solid) with background turbulence excitation parameter  $\varepsilon/\varepsilon_c = 9$ . Symbols are marking intervals of 10 units of time. The metastable state is characterized by  $D/D_c \approx 1.7$ . Parameters as in the previous figures.

that are revealed by S3T analysis give rise to the structure observed in pre-transitional turbulent Couette flow in both NL and ensemble NL simulations. However, the stable S3T modes supported in the S3T stable interval ( $0 < \varepsilon/\varepsilon_c < 1$ ) are also important structures in the dynamics of pre-transitional turbulence. While not excited in the fluctuation free S3T dynamics, these stable S3T modes are robustly excited by fluctuations in the forcing in  $NL_1$  simulations (cf. [38, 39, 44]). Correspondingly, for subcritical excitation ( $0 < \varepsilon/\varepsilon_c < 1$ ) the mean flow of NL or ensemble NL simulations reveals a ubiquitous tendency to form roll/streak structures with temporally variable ( $y, z$ ) structure arising from excitation of the stable manifold of S3T eigenmodes. A POD analysis (cf. [45]) of the streamwise mean flow reveals the dominance of this component of the variability which is accounted for by excitation of these roll/streak structures predicted by S3T (cf. [46]). For example, the first 4 POD's of  $NL_1$  at  $\varepsilon/\varepsilon_c = 0.75$ , shown in Fig. 5, have the structure predicted by the S3T eigenmodes. Consistent with S3T analysis the first POD corresponds to the mode with spanwise wavenumber  $k_z = 4\pi/L_z$ , which corresponds to the least stable eigenfunction at this  $\varepsilon/\varepsilon_c$ . Note that all POD's exhibit exact alignment of the roll circulations with the streaks. This provides confirmation of the S3T prediction that these are the modal structures predicted by S3T. Consistent with these stable modes being excited by turbulent fluctuations, as  $\varepsilon/\varepsilon_c \rightarrow 1$  fluctuations of roll/streak form exhibit enhanced variance (cf.

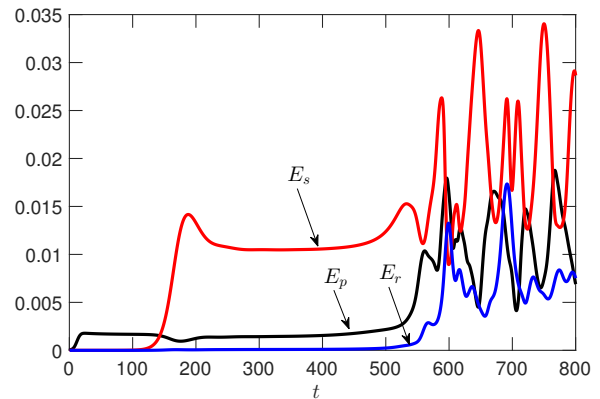


FIG. 7: Evolution of the streak energy,  $E_s$ , roll energy,  $E_r$ , and perturbation energy  $E_p$ , in an S3T integration at  $\varepsilon/\varepsilon_c = 9$  under spanwise homogeneous forcing. The flow is initialized with a small random streamwise mean perturbation with spanwise dependence in order to break spanwise symmetry. The spanwise symmetric S3T equilibrium is unstable and a quasi-steady state emerges by time  $t = 200$  with the roll/streak structure shown in Fig. 8. At this supercriticality the roll/streak structure (cf. Fig. 9) is an unstable fixed point of the S3T dynamics and the flow transitions to the turbulent state. Other parameters as in the previous figures.

Fig. 2) which is indicative of approach to a bifurcation and is a phenomenon analogous to that of critical opalescence on approach to a fluid phase transition.

#### IV. TRANSITION TO TURBULENCE

At background turbulence excitation parameters exceeding  $\varepsilon_t$  ( $\varepsilon_t/\varepsilon_c \approx 5.5$  for the chosen parameters) the finite amplitude roll/streak equilibria are no longer S3T stable and the flow transitions to a turbulent state, which is self-sustaining and persists even when the background turbulence excitation parameter is subsequently set to  $\varepsilon = 0$  (cf. [28]).  $RNL_1$  and  $NL_1$  also transition to essentially similar self-sustaining turbulence. Example trajectories of transition from the laminar equilibrium state to the turbulent attractor for  $NL_1$  and S3T are shown in Fig. 6.

A typical evolution of the perturbation energy density,  $E_p$ , streak energy density,  $E_s$ , and roll energy density,  $E_r$ , of background turbulence excitation parameter  $\varepsilon/\varepsilon_c = 9$  is shown in Fig. 7 for the case of S3T. The S3T integration was initialized with a small random streak perturbation. The flow transitions to turbulence at time  $T \approx 550$ . In this transition process the roll/streak emerges at first as an S3T instability which equilibrates by time  $T \approx 200$  to the quasi-equilibrium finite amplitude roll/streak structure shown in the left panel of Fig. 8. This quasi-equilibrium is associated



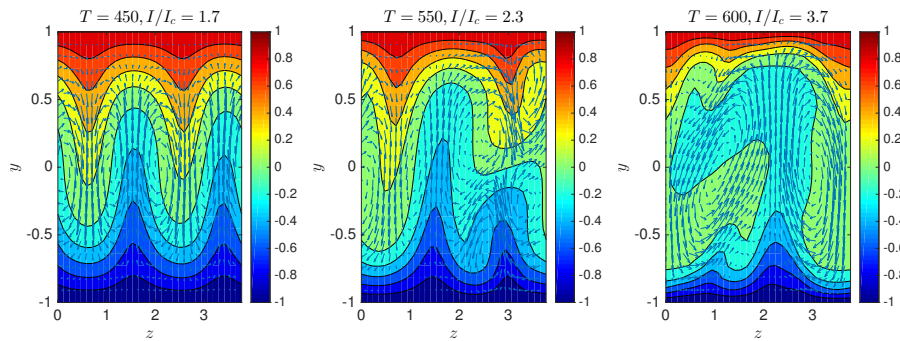


FIG. 8: Snapshots of the streamwise mean flow as it undergoes S3T transition to turbulence under stochastic forcing. Shown are contours of the streak velocity,  $U_s$ , and velocity vectors of the components  $(V, W)$  plotted on the  $(y, z)$  plane. A quasi-steady roll/streak is first formed (cf. left panel) with with input energy rate  $I/I_c \approx 1.7$  and the structure of the fastest growing S3T instability (cf. Fig. 1) which has spanwise wavenumber  $k_z = 4\pi/L_z$ . At about  $t = 550$  the flow transitions through oscillations to a turbulent roll/streak with a dominant  $k_z = 2\pi/L_z$  structure.

The transition period can be extended by enforcing the mirror symmetry of the streak-roll structure about the streak maximum. Other parameters as in the previous figures.

with an energy input-rate  $I/I_c \approx 1.7$ , which lies approximately midway between the value associated with the laminar state and that associated with the statistical mean of the turbulent state. At these parameters there exists near this quasi-equilibrium a symmetric unstable equilibrium, shown in Fig. 9, which can be converged to by suppressing spanwise asymmetries. The roll/streak structure that emerged in the S3T in the presence of realistic spanwise asymmetric perturbations breaks by exciting the unstable directions of the unstable equilibrium at about  $T \approx 550$  and the flow transitions to turbulence. While this pathway to turbulence is typical in all S3T simulations with  $\varepsilon > \varepsilon_t$  the timing of transition depends on the structure of the initialized state which determines the projection on the instability of the S3T equilibrium state. For example, if the flow state at  $\varepsilon/\varepsilon_c = 9$  is constrained to have no perturbations breaking mirror-symmetry in the spanwise direction the flow equilibrates to the unstable roll/streak structure shown in Fig. 9 without ever transitioning to turbulence, while if the initial flow state includes a rich spectrum of such perturbations the meta-stable period is appreciably shortened.

This sequence of events, with rapid break-down of the finite amplitude roll/streak structure, is observed in  $NL_1$  simulations at  $\varepsilon/\varepsilon_c = 9$  when the simulation is initialized with the laminar state. The roll/streak structure associated with the underlying S3T instability arises at first, as in the S3T simulation, but then rapidly transitions to the turbulent state. Snapshots of the roll/streak structure during this transition, which occurs by  $T = 90$ , are shown in Fig. 10.

## V. CONCLUSION

SSD makes available to analysis the manifold of nonlinear instabilities associated with the systematic organiza-

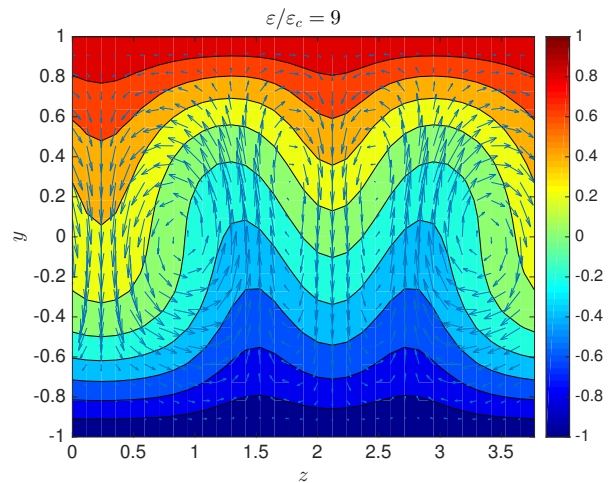


FIG. 9: The unstable roll/streak S3T equilibrium at  $\varepsilon/\varepsilon_c = 9$ . Shown are contours of the streak velocity,  $U_s$ , and velocity vectors of the components  $(V, W)$  plotted on a  $(y, z)$  plane cross-section. Other parameters as in the previous figures.

tion of the background turbulence by coherent structures. In this work the S3T implementation of SSD was used to study instabilities of this type and their nonlinear extensions in a minimal channel configuration of Couette flow. At first a manifold of stable modes with roll/streak form is supported as the parameter controlling the background turbulence intensity,  $\varepsilon$ , is increased from zero. The least stable mode of this manifold is destabilized at a critical excitation designated  $\varepsilon_c$  and a finite amplitude stable fixed point with roll/streak structure arises for excitations between  $\varepsilon_c$  and a second critical value for which the finite amplitude equilibrium roll/streak is destabilized, designated  $\varepsilon_t$ . For excitation exceeding  $\varepsilon_t$  the

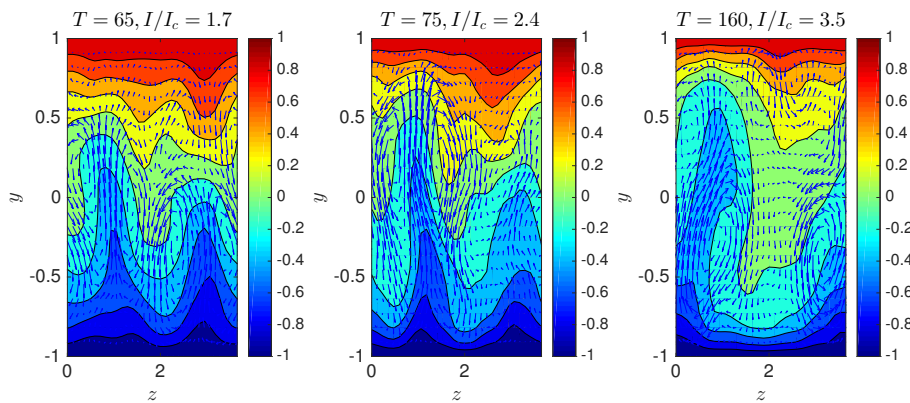


FIG. 10: Snapshots of the streamwise mean flow as it undergoes transition to turbulence in a  $NL_1$  simulation under stochastic forcing, with  $\varepsilon/\varepsilon_c = 9$ . Shown are contours of the streak velocity,  $U_s$ , and velocity vectors of the components  $(V, W)$  in the  $(y, z)$  plane. A quasi-steady roll/streak initially forms, by  $T = 65$ , that swiftly breaks down and the flow transitions to turbulence. The transition is as in the S3T simulation (cf. Fig. 7 and Fig. 8), except that the flow passes through the metastable state rapidly. Other parameters as in the previous figures.

roll/streak equilibrium is unstable to spanwise asymmetric perturbations and becomes time-dependent resulting in the establishment of the turbulent state with spanwise wavenumber approximately half that of the equilibrium state. This sequence of states and transitions suggests a route to turbulence in a developing boundary layer. In order to study these SSD states and their dynamics in more detail their correspondence to realization dynamics was examined making use of a comparison among the predictions of S3T and ensemble implementations of a quasi-linear model sharing the dynamical restrictions of S3T ( $RNL_N$ ) and the associated nonlinear model ( $NL_N$ ). Although the SSD instabilities and their associated fixed point nonlinear equilibria and time dependent statistical mean attractor states have analytical expression only in the S3T implementation of the equivalently infinite ensemble SSD dynamics, the predicted dynamics is clearly reflected in both the dynamically similar quasi-linear system ( $RNL_1$ ) and in DNS ( $NL_1$ ). This correspondence was further examined using ensemble implementations of the RNL and DNS systems. As a consequence of sharing the same dynamical restrictions, the  $RNL_N$  system converges to S3T as  $N \rightarrow \infty$ . Remarkably, the  $NL_N$  system, which corresponds to a full closure for this problem, also

converges to close correspondence with S3T as  $N \rightarrow \infty$ . This convergence is reflected in similar bifurcation behavior as well as similar equilibrium structures for the stable fixed point equilibria. Additionally, S3T also predicts a second bifurcation at a higher value of the turbulent excitation parameter that results in destabilization of the finite amplitude roll/streak equilibria and establishment of a turbulent state corresponding to minimal channel turbulence. This scenario constitutes a mechanism for bypass transition to the turbulent state. Comparison with  $NL_1$  reveals that this mechanism in fact is responsible for bypass transition in the case that the transition is instigated by background turbulence rather than by an optimal perturbation imposed at sufficiently high amplitude.

## ACKNOWLEDGMENTS

Brian Farrell was partially supported by NSF AGS-1246929. We thank Daniel Chung, Navid Constantinou, Dennice Gayme and Vaughan Thomas for helpful discussions.

- 
- [1] P. S. Klebanoff, K. D. Tidstrom, and L. M. Sargent, “The three-dimensional nature of boundary-layer instability,” *J. Fluid Mech.* **12**, 1–34 (1962).
  - [2] S. J. Kline, W. C. Reynolds, F. A. Schraub, and P. W. Runstadler, “The structure of turbulent boundary layers,” *J. Fluid Mech.* **30**, 741–773 (1967).
  - [3] H. P. Bakewell Jr. and L. Lumley, “Viscous sublayer and adjacent wall region in turbulent pipe flow,” *Phys. Fluids* **10**, 1880–1889 (1967).
  - [4] J. Kim, S. J. Kline, and W. C. Reynolds, “The production of turbulence near a smooth wall in a turbulent boundary layers,” *J. Fluid Mech.* **50**, 133–160 (1971).
  - [5] J. Kim, P. Moin, and R. Moser, “Turbulence statistics in fully developed channel flow at low Reynolds number,” *J. Fluid Mech.* **177**, 133–166 (1987).
  - [6] J. Jiménez and P. Moin, “The minimal flow unit in near-wall turbulence,” *J. Fluid Mech.* **225**, 213–240 (1991).
  - [7] K. Hamilton, J. Kim, and F. Waleffe, “Regeneration mechanisms of near-wall turbulence structures,” *J. Fluid*

- Mech.* **287**, 317–348 (1995).
- [8] W. Schoppa and F. Hussain, “Coherent structure generation in near-wall turbulence,” *J. Fluid Mech.* **453**, 57–108 (2002).
  - [9] J. Jiménez, “Near-wall turbulence,” *Phys. Fluids* **25**, 101302 (2013).
  - [10] Y. Hwang and C. Cossu, “Self-sustained processes in the logarithmic layer of turbulent channel flows,” *Phys. Fluids* **23**, 061702 (2011).
  - [11] B. F. Farrell, P. J. Ioannou, J. Jiménez, N. C. Constantinou, A. Lozano-Durán, and M.-A. Nikolaidis, “A statistical state dynamics-based study of the structure and mechanism of large-scale motions in plane Poiseuille flow,” *J. Fluid Mech.* **809**, 290–315 (2016).
  - [12] T. Ellingsen and E. Palm, “Stability of linear flow,” *Phys. Fluids* **18**, 487–488 (1975).
  - [13] M. T. Landahl, “A note on an algebraic instability of inviscid parallel shear flows,” *J. Fluid Mech.* **98**, 243–251 (1980).
  - [14] B. F. Farrell and P. J. Ioannou, “Generalized stability. Part I: Autonomous operators,” *J. Atmos. Sci.* **53**, 2025–2040 (1996).
  - [15] B. F. Farrell and P. J. Ioannou, “Generalized stability. Part II: Non-autonomous operators,” *J. Atmos. Sci.* **53**, 2041–2053 (1996).
  - [16] P. J. Schmid and D. S. Henningson, *Stability and Transition in Shear Flows* (Springer, New York, 2001).
  - [17] K. M. Butler and B. F. Farrell, “Three-dimensional optimal perturbations in viscous shear flows,” *Phys. Fluids* **4**, 1637–1650 (1992).
  - [18] S. C. Reddy and D. S. Henningson, “Energy growth in viscous channel flows,” *J. Fluid Mech.* **252**, 209–238 (1993).
  - [19] M. R. Head and I. Rechenberg, “The Preston tube as a means of measuring skin friction,” *J. Fluid Mech.* **14**, 1–17 (1962).
  - [20] P. Bradshaw, “The effect of wind-tunnel screens on nominally two-dimensional boundary layers,” *J. Fluid Mech.* **22**, 679–687 (1965).
  - [21] A. A. Townsend, *The structure of turbulent shear flow*, 2nd ed. (Cambridge University Press, 1976).
  - [22] A. A. Bakchinov, M. M. Katasonov, and V. V. Kozlov, “Experimental study of localized disturbances and their development in a flat plate boundary layer,” Preprint No. 1-97, ITAM, Russian Academy of Sciences, Novosibirsk, Russia (in Russian) (1997).
  - [23] P. H. Alfredsson and M. Matsubara, “Streaky structures in transition,” in *Proc. Transitional Boundary Layers in Aeronautics*, edited by R. A. W. M. Henkes and J. L. van Ingen (Royal Netherlands Academy of Arts and Sciences. Elsevier Science Publishers, 1996) pp. 373–386.
  - [24] K. J. A. Westin, A. A. Bakchinov, V. V. Kozlov, and P. H. Alfredsson, “Experiments on localized disturbances in a flat plate boundary layer. Part 1. The receptivity and evolution of a localized free stream disturbance,” *Eur. J. Mech. B-Fluid* **17**, 823–846 (1998).
  - [25] K. J. A. Westin, A. V. Boiko, B. G. B. Klingmann, V. V. Kozlov, and P. H. Alfredsson, “Experiments in a boundary layer subjected to free stream turbulence. Part 1. Boundary layer structure and receptivity,” *J. Fluid Mech.* **281**, 193–218 (1994).
  - [26] L. N. Trefethen, A. E. Trefethen, S. C. Reddy, and T. A. Driscoll, “Hydrodynamic stability without eigenvalues,” *Science* **261**, 578–584 (1993).
  - [27] L. N. Trefethen and M. Embree, *Spectra and Pseudospectra: The Behavior of Nonnormal Matrices and Operators* (Princeton University Press, Princeton, 2005).
  - [28] B. F. Farrell and P. J. Ioannou, “Dynamics of streamwise rolls and streaks in turbulent wall-bounded shear flow,” *J. Fluid Mech.* **708**, 149–196 (2012).
  - [29] N. C. Constantinou, B. F. Farrell, and P. J. Ioannou, “Statistical state dynamics of jet–wave coexistence in barotropic beta-plane turbulence,” *J. Atmos. Sci.* **73**, 2229–2253 (2016).
  - [30] V. Thomas, B. K. Lieu, M. R. Jovanović, B. F. Farrell, P. J. Ioannou, and D. F. Gayme, “Self-sustaining turbulence in a restricted nonlinear model of plane Couette flow,” *Phys. Fluids* **26**, 105112 (2014).
  - [31] M. Nagata, “Three-dimensional traveling-wave solutions in plane Couette flow,” *Phys. Rev. E* **55**, 2023–2025 (1997).
  - [32] P. Hall and F. Smith, “On strongly nonlinear vortex/wave interactions in boundary-layer transition,” *J. Fluid Mech.* **227**, 641–666 (1991).
  - [33] F. Waleffe, “Homotopy of exact coherent structures in plane shear flows,” *Phys. Fluids* **15**, 1517–1534 (2003).
  - [34] J. Wang, J. Gibson, and F. Waleffe, “Lower branch coherent states in shear flows: Transition and control,” *Phys. Rev. Lett.* **98**, 204501 (2007).
  - [35] K. Deguchi, P. Hall, and A. Walton, “The emergence of localized vortex-wave interaction states in plane Couette flow,” *J. Fluid Mech.* **721**, 58–85 (2013).
  - [36] K. Deguchi and P. Hall, “The high-Reynolds-number asymptotic development of nonlinear equilibrium states in plane Couette flow,” *J. Fluid Mech.* **750**, 99–112 (2014).
  - [37] K. Deguchi and P. Hall, “On the instability of vortex-wave interaction states,” *J. Fluid Mech.* **802**, 634–666 (2016).
  - [38] B. F. Farrell and P. J. Ioannou, “Structural stability of turbulent jets,” *J. Atmos. Sci.* **60**, 2101–2118 (2003).
  - [39] B. F. Farrell and P. J. Ioannou, “Statistical State Dynamics: a new perspective on turbulence in shear flow,” in *Zonal jets*, edited by B. Galperin and P. L. Read (Cambridge University Press, 2016) Chap. 5, (submitted, arXiv:1412.8290).
  - [40] P. Hall and S. Sherwin, “Streamwise vortices in shear flows: harbingers of transition and the skeleton of coherent structures,” *J. Fluid Mech.* **661**, 178–205 (2010).
  - [41] A. Eliassen and E. Palm, “On the transfer of energy in stationary mountain waves,” *Geophys. Publ.* **XXII**, 1–23 (1961).
  - [42] J. P. Boyd, “The noninteraction of waves with the zonally averaged flow on a spherical Earth and the interrelationships on eddy fluxes of energy, heat and momentum,” *J. Atmos. Sci.* **33**, 2285–2291 (1976).
  - [43] D. G. Andrews and M. E. McIntyre, “Planetary waves in horizontal and vertical shear: The generalized Eliassen-Palm relation and the mean zonal acceleration,” *J. Atmos. Sci.* **33**, 2031–2048 (1976).
  - [44] N. C. Constantinou, B. F. Farrell, and P. J. Ioannou, “Emergence and equilibration of jets in beta-plane turbulence: applications of Stochastic Structural Stability Theory,” *J. Atmos. Sci.* **71**, 1818–1842 (2014).
  - [45] G. Berkooz, P. Holmes, and J. L. Lumley, “The proper orthogonal decomposition in the analysis of turbulent flows,” *Annu. Rev. Fluid Mech.* **25**, 539–575 (1993).

- [46] M.-A. Nikolaidis, B. F. Farrell, P. J. Ioannou, D. F. Gayme, A. Lozano-Durán, and J. Jiménez, “A POD-based analysis of turbulence in the reduced nonlinear dynamics system.” *J. Phys.: Conf. Ser.* **708**, 012002 (2016).